Available online at www.sciencedirect.com
ScienceDirect
International Journal of Thermal Sciences 46 (2007) 662–671
International Journal of Thermal Sciences
www.elsevier.com/locate/ijts

Numerical simulation of combined thermal and mass transport in a square lid-driven cavity

Abdalla M. Al-Amiri [a], Khalil M. Khanafer [b,*], Ioan Pop [c]

[a] *Mechanical Engineering Department, United Arab Emirates University, PO Box 17555 Al-Ain, United Arab Emirates*
[b] *Biomedical Engineering Department, University of Michigan, Ann Arbor, MI 48109, USA*
[c] *Faculty of Mathematics, University of Cluj, R-3400 Cluj, Romania*

Received 5 January 2006; received in revised form 31 August 2006; accepted 11 October 2006

Available online 20 November 2006

Abstract

The aim of this study was to investigate steady mixed convection in a square lid-driven cavity under the combined buoyancy effects of thermal and mass diffusion. The transport equations were solved numerically using the Galerkin weighted residual method. The heat and mass transfer rates were examined using several operational dimensionless parameters, such as the Richardson number Ri, Lewis number Le and buoyancy ratio parameter N. The investigation was carried out for $4 \times 10^{-4} \leqslant Ri \leqslant 10$, $1 \leqslant Le \leqslant 50$ and $-100 \leqslant N \leqslant 100$. Domains of high transport phenomena were identified and highlighted. Furthermore, the average Nusselt and Sherwood numbers are obtained at the bottom wall for some values of the parameters considered in this investigation. The results demonstrate the range where high heat and mass transfer rates can be attained for a given Richardson number. This paper fills the gap by considering the combined heat and mass transfer by mixed convection for the classical problem of a lid-driven cavity flow.

Keywords: Lid-driven cavity flows; Thermal and mass diffusion; Numerical study

1. Introduction

In nature and in many engineering applications there are many transport processes which are governed by the combined action of the buoyancy forces from both thermal and mass (concentration) processes. Representative fields of interest include spray and flash drying, combustion of atomized liquid fuels, cyclone evaporation and drying and dehydration operations in chemical and food processing plants, crystal growth, material and separation processes, etc. [1]. The modern technologies require thorough understanding of the pertinent processes involved in these fields. Considerable research work has been reported in the literature on natural convection due to combined thermal and mass (concentration) buoyancy forces. Unfortunately, pure natural or pure forced convection situations seldom arise in practice. Often the practical processes are governed by the combined action of natural and forced convection and, depending on the situation; one may predominate over the other. The orientation of the cavity with respect to the gravitational field, for instance, provides various scenarios depending whether the density gradient is parallel or perpendicular to gravity vector. Ostrach [2] provided physical insights into a cavity filled with a binary fluid that is subjected to a combined buoyancy driving force. Mohamad and Viskanta [3] predicted the flow and heat transfer in a shallow, lid-driven cavity with a low Prandtl number fluid. They considered the cavity to be either heated from bellow or heated from above. Further, Ben Mansour and Viskanta [4] presented both experimental and theoretical studies on mixed convection heat transfer in a shallow cavity with a moving bottom wall. Aydin [5] conducted a numerical study to investigate the transport mechanism of laminar mixed convection in a shear- and buoyancy-driven cavity. Two orientations of thermal boundary conditions at the cavity walls were considered to simulate the aiding- and opposing-buoyancy mechanism. Hsu et al. [6] have numerically investigated laminar mixed convection flow of micropolar fluids in a lid-driven

* Corresponding author. Tel.: +1(734) 763 5240.
E-mail addresses: alamiri@uaeu.ac.ae (A.M. Al-Amiri), khanafer@umich.edu (K.M. Khanafer), popi@math.ubbcluj.ro (I. Pop).

1290-0729/$ – see front matter
doi:10.1016/j.ijthermalsci.2006.10.003

Nomenclature

C	species mass fraction or concentration
D	binary diffusion coefficient
g	gravitational acceleration
Gr_S	Grashof number due to mass diffusion, $g\beta_S(C_{\text{hot}} - C_{\text{cold}})H^3/\upsilon^2$
Gr_T	Grashof number due to thermal diffusion, $g\beta_T(T_{\text{hot}} - T_{\text{cold}})H^3/\upsilon^2$
H	height of cavity
L	length of cavity
Le	Lewis number, Sc/Pr
N	buoyancy ratio parameter, Gr_S/Gr_T
Nu	average Nusselt number
P	dimensionless pressure
Pr	Prandtl number, υ/α
Re	Reynolds number, U_0H/υ
Ri	Richardson number, Gr_T/Re^2
S	source term appearing in Eq. (18)
Sc	Schmidt number, υ/D
Sh	average Sherwood number
t	time
T	temperature
u, v	velocity components along x- and y-axes
U, V	dimensionless velocity components
U_0	top wall velocity
x, y	Cartesian coordinates along the lower and upper walls, respectively
X, Y	dimensionless coordinates

Greek symbols

α	thermal diffusivity
β_C	volumetric coefficient of expansion with mass fraction
β_T	volumetric coefficient of thermal expansion
Λ	dependant variable appearing in Eq. (18)
υ	fluid kinematic viscosity
Φ	dimensionless mass (concentration) diffusion, $(C - C_{\text{cold}})/(C_{\text{hot}} - C_{\text{cold}})$
θ	dimensionless temperature, $(T - T_{\text{cold}})/(T_{\text{hot}} - T_{\text{cold}})$
ϑ	diffusion coefficient appearing in Eq. (18)
ρ	density
ρ_0	characteristic density
τ	dimensionless time, tU_0/H
Ω	dimensionless vorticity, $\omega H/U_0$
Ψ	dimensionless stream function, ψ/HU_0

Subscripts

cold	top wall
hot	bottom wall

cavity. Aydin and Yang [7] conducted a numerical study to investigate the transport mechanism of mixed convection in a shear- and buoyancy-driven cavity having a locally heated lower wall and moving cooled sidewalls. In the work of Trevisan and Bejan [8], scaling analysis was used to show mass transfer dependency in a cavity. They have also determined analytically mass transfer rate at high Reynolds number in a thermally driven environment. In addition, several experimental [9,10] and numerical [11–13] investigations were carried out in this regard. Weaver and Viskanta [14] have shown experimentally natural convection in binary gases due to horizontal thermal and solutal gradients in enhancing and opposing flow situations.

It appears from the literature review that the combination of heat and mass transfer in lid-driven enclosures has received less attention. In drying technology, better understanding of the drying process is vital for optimum performance of the drying chamber. A typical drying chamber can be modeled as a cavity with both temperature and concentration gradients being present to allow the transfer of moisture, for example. In such situations, heat is applied to the bottom wall to simulate the evaporation of the liquid solvent while the top surface is cooled such that the solvent vapor condenses on it. Thus, the undesired concentration (i.e. solvent vapor) can be removed by a mechanically-induced conveyor belt. Therefore, the combination of buoyancy effect by temperature and concentration lead to complicated flow patterns in the drying chamber which significantly influence the heat and mass transfer rates (solvent evaporation rate) inside the cavity.

Kuhlmann et al. [15] has studied thermal and mass transport in tangentially opposing cavity walls. Moreover, Alleborn et al. [16] have numerically investigated the behavior of a shallow cavity under thermosolutal boundary conditions. They have reported that the cavity orientation becomes insignificant should the lid speed increase substantially. Stable operating condition was achieved at high mass transfer rates. On the contrary, instabilities were observed when the forced convection effect was depreciated. What is more, ranges of minimum heat and mass transfer were identified for different configurations of thermal and solutal density changes.

To the best knowledge of the present authors, no attention has been paid to the problem of mixed convection in a lid-driven cavity under the combined buoyancy effects of thermal and mass (species) diffusion. The bottom-heated wall is considered the source while the top wall is taken as the product, where material of the fluid is deposited and removed by the moving top wall in the horizontal plane. In the current investigation, the transport phenomena will be explored by utilizing several key operational dimensionless parameters. These parameters are the Richardson number, Lewis number and the concentration-to-thermal buoyancy ratio, namely, the buoyancy ratio number. These parameters will be examined over a broad range to study their implications on the mass and energy transport phenomena in the cavity.

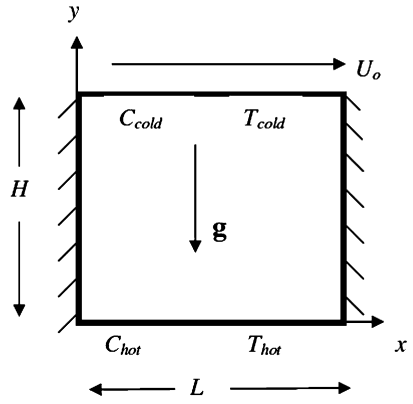

Fig. 1. Physical model and coordinate system.

2. Mathematical model

The physical system considered in the present study is presented in Fig. 1. A two-dimensional cavity of height H and length L is filled with an incompressible Newtonian perfect mixture of a binary fluid that operates in the laminar regime under steady state conditions. The vertical walls are considered adiabatic and impermeable. In addition, the horizontal walls are maintained at uniform but different temperatures and concentrations such that the bottom wall has the temperature T_{hot} and concentration C_{hot}, while the top wall has the temperature T_{cold} and concentration C_{cold}, where $T_{\text{hot}} > T_{\text{cold}}$ and $C_{\text{hot}} > C_{\text{cold}}$, respectively. The walls can be viewed as walls with infinite heat and mass diffusivities. Moreover, the top-cold wall is assumed to slide from left to right at a constant speed U_0. The fluid properties are assumed constant except for the density ρ, which is assumed to vary linearly with both temperature and concentration [14,17–21] and is given by $\rho = \rho_0[1 - \beta_T(T - T_{\text{cold}}) - \beta_C(C - C_{\text{cold}})]$, where ρ_0 is a characteristic density, and β_T and β_C are volumetric expansion coefficients with temperature and mass (concentration) fraction, respectively. In the present study, β_T is considered as positive, while β_C can be either positive or negative with $\beta_C > 0$ for cooperative flows and $\beta_C < 0$ for opposing flows, respectively. Furthermore, the Soret and Duffor effects are assumed to be negligible in this study. The governing equations were presented in dimensionless form using the following new variables:

$$X = \frac{x}{H}, \qquad Y = \frac{y}{H}, \qquad \tau = \frac{tU_0}{H}$$
$$\theta = \frac{T - T_{\text{cold}}}{T_{\text{hot}} - T_{\text{cold}}}, \qquad \Phi = \frac{C - C_{\text{cold}}}{C_{\text{hot}} - C_{\text{cold}}} \tag{1}$$

where x and y are the Cartesian coordinates measured along the horizontal and vertical walls, respectively, T is the fluid temperature, C is the species mass fraction or concentration, t is the time, θ is the dimensionless temperature and Φ is the dimensionless mass or concentration fraction. The dimensionless forms of the governing equations in the binary fluid are expressed in the following canonical forms:

$$\nabla.\mathbf{V} = 0 \tag{2}$$

$$\frac{\partial \mathbf{V}}{\partial \tau} + (\mathbf{V}.\nabla)\mathbf{V} = \frac{1}{Re}\nabla^2\mathbf{V} + \frac{Gr_T}{Re^2}\left(\theta + \frac{Gr_S}{Gr_T}\Phi\right) - \frac{\nabla P}{Re} \tag{3}$$

$$\frac{\partial \Phi}{\partial \tau} + \mathbf{V}.\nabla\Phi = \frac{1}{Sc\,Re}\nabla^2\Phi \tag{4}$$

$$\frac{\partial \theta}{\partial \tau} + \mathbf{V}.\nabla\theta = \frac{1}{Pr\,Re}\nabla^2\theta \tag{5}$$

where $\mathbf{V}$ is the velocity vector, P is the dimensionless pressure, $Re = U_0H/\upsilon$ is the Reynolds number, $Sc = \upsilon/D$ is the Schmidt number, while $Gr_T = g\beta_T(T_{\text{hot}} - T_{\text{cold}})H^3/\upsilon^2$ and $Gr_S = g\beta_C(C_{\text{hot}} - C_{\text{cold}})H^3/\upsilon^2$ are the thermal and solutal Grashof numbers, respectively. Also g is the gravity acceleration, υ is the kinematic viscosity and D is the solutal (concentration) diffusivity. By introducing of new variables, namely the vorticity and the stream function, the Navier–Stokes equations are decoupled into one elliptic equation and one parabolic equation which can be solved sequentially. However, the governing equations are a mixed elliptic–parabolic system of equations which need to be solved simultaneously in case of primitive variables formulation. Upon invoking the vorticity-stream function formulations represented by

$$U = \frac{\partial \Psi}{\partial Y}, \qquad V = -\frac{\partial \Psi}{\partial X}, \qquad \Omega = \frac{\partial V}{\partial X} - \frac{\partial U}{\partial Y} \tag{6}$$

$$\Omega = -\nabla^2\Psi \tag{7}$$

we obtain the following dimensionless equations:

$$\frac{\partial \Omega}{\partial \tau} + \left(U\frac{\partial \Omega}{\partial X} + V\frac{\partial \Omega}{\partial Y}\right) = \frac{1}{Re}\left(\frac{\partial^2\Omega}{\partial X^2} + \frac{\partial^2\Omega}{\partial Y^2}\right) + Ri^2\left(\frac{\partial \theta}{\partial X} + N\frac{\partial \Phi}{\partial X}\right) \tag{8}$$

$$\frac{\partial \Phi}{\partial \tau} + \left(U\frac{\partial \Phi}{\partial X} + V\frac{\partial \Phi}{\partial Y}\right) = \frac{1}{Re\,Sc}\left(\frac{\partial^2\Phi}{\partial X^2} + \frac{\partial^2\Phi}{\partial Y^2}\right) \tag{9}$$

$$\frac{\partial \theta}{\partial \tau} + \left(U\frac{\partial \theta}{\partial X} + V\frac{\partial \theta}{\partial Y}\right) = \frac{1}{Re\,Pr}\left(\frac{\partial^2\theta}{\partial X^2} + \frac{\partial^2\theta}{\partial Y^2}\right) \tag{10}$$

where $Ri = Gr_T/Re^2$ is the Richardson number. Here the dimensionless velocity components U and V, the stream function Ψ and vorticity Ω are defined as:

$$U = \frac{u}{U_0}, \qquad V = \frac{v}{U_0}, \qquad \Omega = \frac{\omega H}{U_0}, \qquad \Psi = \frac{\psi}{HU_0} \tag{11}$$

with u and v being the dimensional velocity components along x and y axes, ω is the dimensional vorticity and ψ is the dimensional stream function. The buoyancy ratio number N that appears in Eq. (8) represents the ratio of the buoyancy forces due to solutal (concentration) gradients to temperature gradients such that

$$N = \frac{\beta_C(C_{\text{hot}} - C_{\text{cold}})}{\beta_T(T_{\text{hot}} - T_{\text{cold}})} = \frac{Gr_S}{Gr_T} \tag{12}$$

where $N > 0$ for aiding flows (counterclockwise direction) and $N < 0$ for opposing flows (clockwise direction), respectively. The initial conditions can be expressed as:

$$\tau = 0: \quad \Psi = \theta = \Phi = 0 \tag{13}$$

and the boundary conditions can be summarized as follows ($\tau > 0$):

$$U = V = 0, \quad \theta = \Phi = 1 \quad \text{at } Y = 0,\ 0 < X < 1$$
$$U = 1, \quad V = 0, \quad \theta = \Phi = 0 \quad \text{at } Y = 1,\ 0 < X < 1$$
$$U = V = 0, \quad \frac{\partial\theta}{\partial X} = \frac{\partial\Phi}{\partial X} = 0 \quad \text{at } X = 0,\ 0 \leqslant Y \leqslant 1$$
$$U = V = 0, \quad \frac{\partial\theta}{\partial X} = \frac{\partial\Phi}{\partial X} = 0 \quad \text{at } X = 1,\ 0 \leqslant Y \leqslant 1 \tag{14}$$

The vorticity on the boundaries is expressed in terms of the primitive velocity variables as

$$\Omega = \frac{\partial V}{\partial X} \quad \text{at } Y = 0, 1; 0 < X < 1$$
$$\Omega = -\frac{\partial U}{\partial Y} \quad \text{at } X = 0, 1; 0 \leqslant Y \leqslant 1 \tag{15}$$

Unsteady governing equations were solved until steady-state solution is achieved. The time step of 10^{-3} was used in this work. The rate of heat and mass transfer are presented in this work at the bottom wall when the solution achieved steady-state condition in terms of Nusselt number *Nu* (dimensionless heat flux) and Sherwood number *Sh* (dimensionless mass flux), respectively as:

$$Nu = \int_0^1 -\frac{\partial\theta}{\partial Y}\bigg|_{Y=0} dX \tag{16}$$

$$Sh = \int_0^1 -\frac{\partial\Phi}{\partial Y}\bigg|_{Y=0} dX \tag{17}$$

It is assumed that the working fluid has a Prandtl number of unity, i.e., $Pr = 1$. This value is chosen to simulate a practical value used in drying technology [16]. Also, since the Lewis number *Le* is defined as $Le = Sc/Pr$, the investigation will consider *Le* as an operational dimensionless parameter instead of *Sc*. In addition, we shall consider here only the case of a cavity ($H = L$).

3. Numerical solution

The governing equations, Eq. (7)–(10), were written in canonical form as:

$$\frac{\partial\Lambda}{\partial\tau} + \frac{\partial(U\Lambda)}{\partial X} + \frac{\partial(V\Lambda)}{\partial Y} = \vartheta\left(\frac{\partial^2\Lambda}{\partial X^2} + \frac{\partial^2\Lambda}{\partial Y^2}\right) + S \tag{18}$$

where Λ is the dependent variable, ϑ is the diffusion coefficient and *S* is the source term. The numerical procedure used in this work is based on the Galerkin weighted residual method of finite-element formulation. The application of this technique is well described by Taylor and Hood [22] and Gresho et al. [23]. The objective of the finite element method is to reduce the continuum problem to a discrete problem described by a system of algebraic equations. The finite element procedure begins with the division of the continuum region of interest into a number of simply shaped regions called elements. These elements were assumed to be fixed in the space. Within each element, the dependent variables are approximated using interpolation functions. Variable grid size system is implemented in the present investigation especially near the walls to capture the rapid changes in the dependent variables. The following enforced convergence criterion was employed in this study to ensure the convergence of the dependent variables

$$\frac{\|\Lambda^{n+1} - \Lambda^n\|_\infty}{\|\Lambda^{n+1}\|_\infty} \leqslant 10^{-5} \tag{19}$$

where *n* is the time index. The overall thermal and mass balances were monitored inside the cavity and both results agreed to within 10^{-5} at the highest value of the Grashof number considered.

4. Results and discussion

4.1. Algorithm validation

The algorithm validation was carried out in two folds. First, grid sensitivity tests were performed to inspect the field variables grid-independency solutions. Uniform node points of 21×21, 41×41, 61×61, 81×81 and 91×91 were examined for $Re = 500$, $Le = 2.0$ and $Gr_S = Gr_T = 10^2$ ($N = 1$). As shown in Fig. 2, adequate results can be achieved using node points of 91×91. To check the accuracy of the present results, our code was validated against published results in the literature on lid-driven cavity flow as shown in Tables 1 and 2. Table 1 illustrates a comparison of the stream function values at the primary vortex location computed for various Reynolds numbers between the present work and several other numerical solutions. Table 2 shows a comparison of the maximum *U*- and *V*-velocity and their locations through the centerlines of the cavity for $Re = 100$. Both tables demonstrate an excellent agreement between our results and other results. An additional check on the accuracy of the present numerical code, Fig. 3 shows a comparison of the *U*-velocity along the vertical mid-section of the cavity between the present results and that of Ghia et al. [26] and both results are in excellent agreement. To further check the accuracy of the present numerical method, the present results were compared with the experimental and numerical results of Weaver and Viskanta [14] as illustrated in Fig. 4. It can

Table 1
Primary vortex stream function value

Re	ψ (Present work)	ψ [24]	ψ [25]	ψ [26]
100	−0.1033	−0.1033	−0.1033	−0.103423
400	−0.1139	−0.11389	−0.11297	−0.113909

Table 2
Extrema of the velocity through the centerlines of the cavity, $Re = 100$

Reference	U_{max}[a]	Y_{max}	V_{max}	X_{max}
Present	0.2120	0.453	0.1788	0.765
[27]	0.21404	0.4581	0.17957	0.7630
[28]	0.21315	–	0.17896	–
[29]	0.2109	0.4531	0.17527	0.7656
[26]	0.2106	0.4531	0.1786	0.7656

[a] The maximum of *U* on the vertical line $X = 0.5$ is denoted U_{max} and its location Y_{max}. The maximum of *V* on the horizontal line $Y = 0.5$ is denoted V_{max} and its location X_{max}.

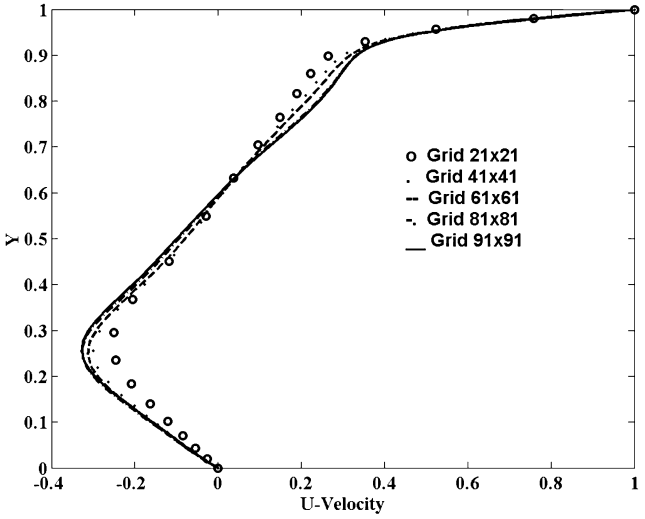

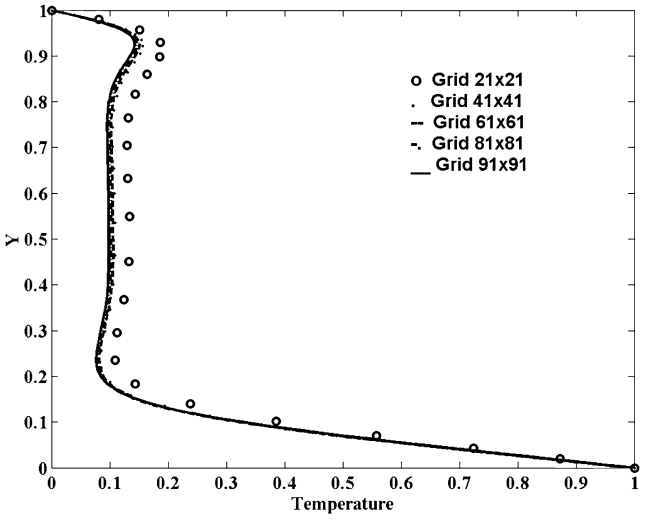

Fig. 2. Grid independence test for $Re = 500$, $Le = 2.0$ and $Gr_S = Gr_T = 10^2$.

be seen from this figure that the results of the present numerical code is in a very good agreement with the numerical and experimental results of Weaver and Viskanta [14] for Grashof numbers of $Gr_T = 5.88 \times 10^5$ and 9.31×10^5 and buoyancy ratios of $N = 0.55$ (aiding flow) and $N = -1.85$ (opposing flow).

4.2. Field variable presentation

The effect of the Richardson number *Ri*, Lewis number *Le* and buoyancy ratio parameter *N* on the steady-state streamline, temperature and concentration distributions as well as the average Nusselt and Sherwood numbers (*Nu* and *Sh*) are presented in the subsequent sections. The maximum and minimum recirculation intensity levels were documented for the presented streamline results.

4.2.1. Effect of Richardson number

The influence of varying the Richardson number *Ri* on the transport phenomena is shown in Fig. 5. The Richardson number provides a measure for the importance of the thermal natural convection relative to the lid-driven forced convection effect.

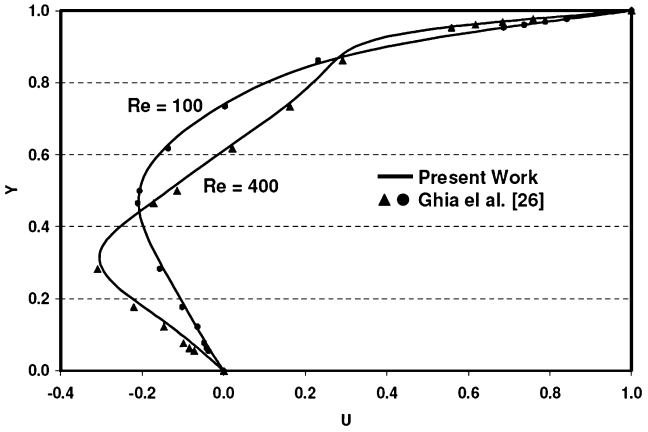

Fig. 3. Comparison of the present predictions to the FV code for $Re = 500$, $Le = 2.0$, and $Gr_S = Gr_T = 10^2$ $(N = 1)$.

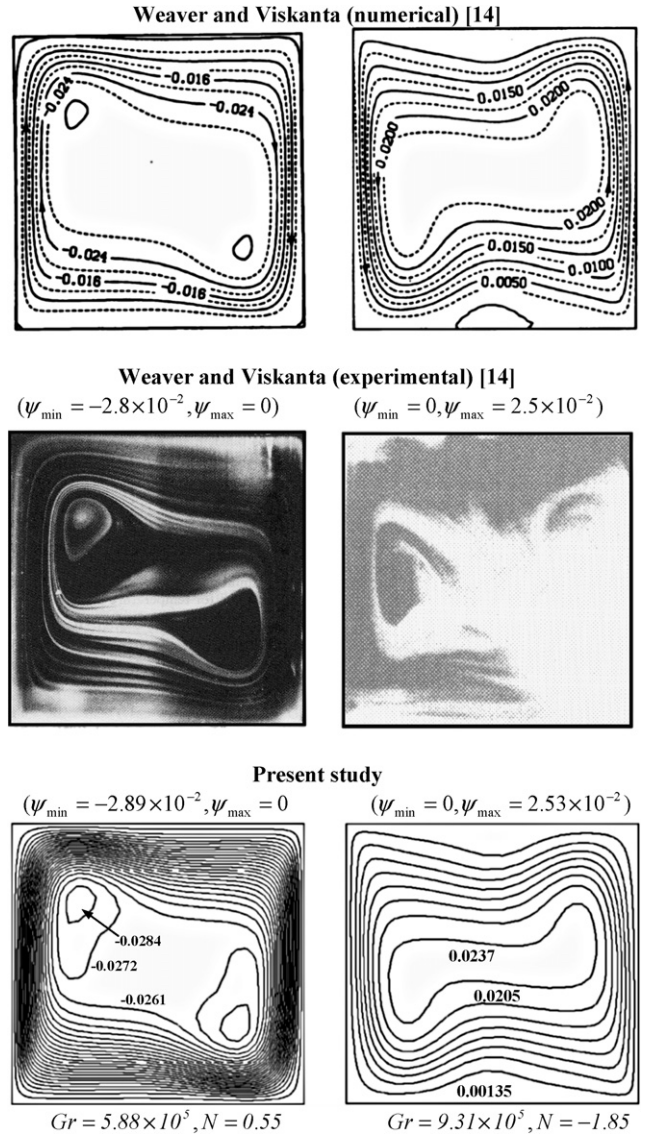

Fig. 4. Comparison of the streamlines between the present numerical solution and that of Weaver and Viskanta [14].

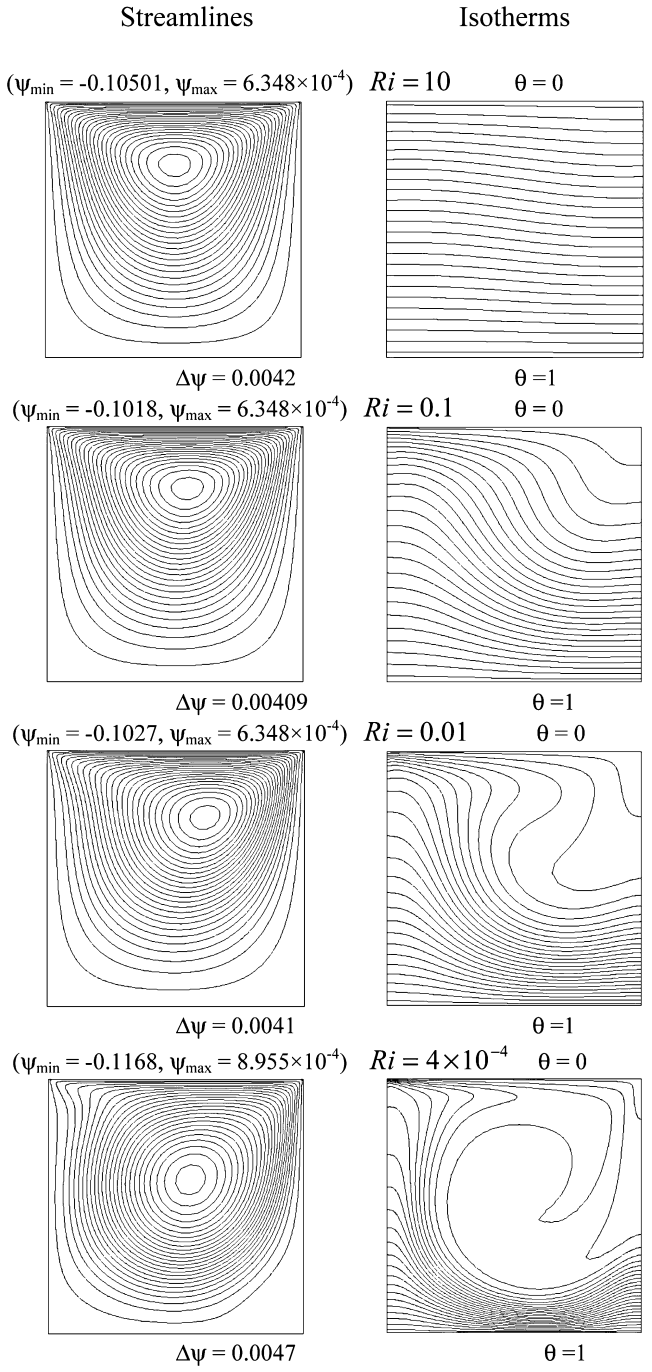

Fig. 5. Effect of Richardson number on the streamlines and isotherms for $Le = 1.0$ and $Gr_S = Gr_T = 10^2$.

The Schmidt number was set to unity ($Sc = 1$), and since $Pr = 1$ then $Le = 1$. This implies similar diffusion characteristics for both heat and mass transfer. Moreover, setting Le to unity will also facilitate highlighting the implications of Ri alone. The value of Ri was varied between 4×10^{-4} to 10, which covers a wide range of operating conditions. For $Ri = 10$, flow patterns are characterized by a primary recirculating clockwise vortex ($N < 0$) that occupies the bulk of the cavity. In addition, minor vortices tend to form near the bottom corners, which maybe captured by increasing the number of contour lines. Furthermore, this configuration is an ingredient for a vertical stratification to be maintained in the entire cavity. It basically implies that the cavity is in a quasi-conduction domain, i.e., most of the heat transfer occurs due to conduction except near the sliding top wall.

Upon decreasing the Ri value to 0.1, the forced convection regime gains more ground over its conduction counterpart. Moreover, the overall flow patterns remain quite the same with a slight reduction in its intensity level (note the drop in the absolute value of Ψ_{max} between $Ri = 10$ and $Ri = 4 \times 10^{-4}$). Also, thinner boundary layers are depicted to form upon further decrease in Ri value. This is attributed to the increase in the contribution of convection heat transfer mechanism, which causes steep temperature gradients in the vertical direction near the bottom wall. Apparently, the buoyancy forces are overwhelmed by the mechanical effect induced by the moving lid (note the increase in the absolute values of both Ψ_{max} and Ψ_{min}). The increase in convection activities escalates the mass transfer rate, i.e., enhanced evaporation rate, which is encouraged if drying conditions are sought. It is important to mention that the mass transfer rate undergoes similar observations to those for heat transfer since $Le = 1$.

4.2.2. *Effect of Lewis number*

The dependence of heat and mass transport on the Sherwood number is demonstrated in Fig. 6. The Lewis number Le was varied between 5 and 50, while Ri was fixed at 0.01 and $N = 1$. The results illustrate significant variations in the mass (concentration) contours owing to the depreciation in the diffusivity value of the mass species upon increasing the values of Le. Thinner mass (concentration) boundary layers are shown to form along the bottom wall, which signals continuous increase in the mass transfer rate with the increase of Le. The results show that much of the mass diffusion occurs between $Le = 5$–25 for $Ri = 0.01$. It is worth noting that the above stated Le range would be either extended or shortened upon further reduction or elevation in the Ri value, respectively. The results also point out that the effect of the Lewis number on the isotherms and streamlines seems to be insignificant as shown in Fig. 6. This is likely to be attributed to the fact that the combined buoyancy effects are very much dominated by the sliding top wall.

4.2.3. *Effect of the buoyancy ratio number*

The effect of the buoyancy ratio parameter N on the streamline and isotherm patterns for a Lewis number of unity ($Le = 1$) is shown in Figs. 7 and 8. The Re and Ri values were fixed at 100 and 0.01, respectively. The parameter N was set to vary between 0–100. When $N = 0$, the mass (concentration) transport phenomenon vanishes and the problem reduces to a pure thermal convection with a heated bottom wall. Further, it can be deduced from Eq. (8) an effective Richardson number which can be defined as $Ri^* = (1 + N)Ri$. Hence, rapid escalation in Ri^* value would be attained for increased N values. The results displayed in Fig. 7 confirm such conclusions, which are visualized by the formation of thinner thermal boundary layer along the bottom wall for higher N values. Consequently, higher tem-

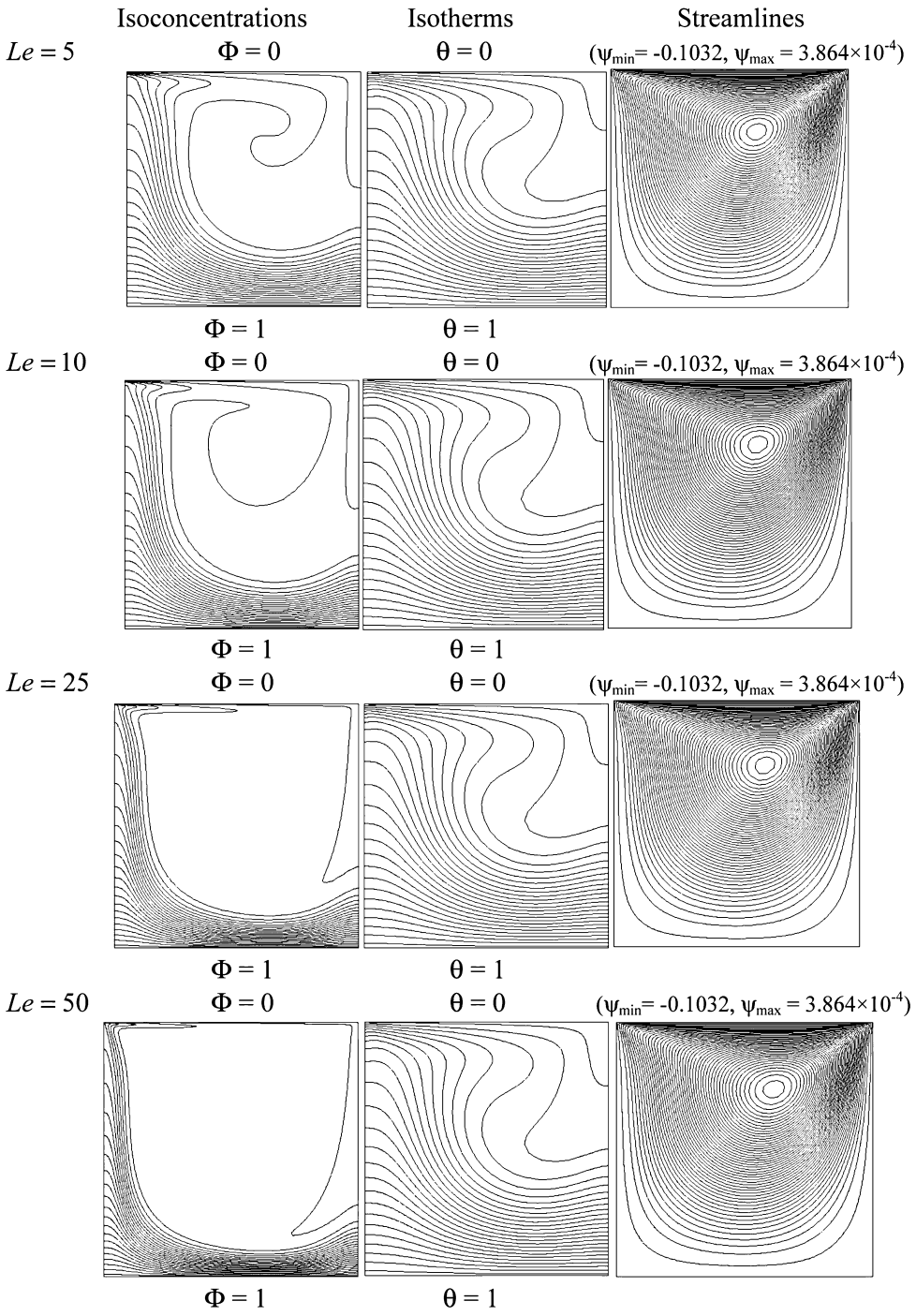

Fig. 6. Effect of Lewis number on the isoconcentrations, isotherms and streamlines for $Re = 100$, $Ri = 0.01$ and $N = 1$.

perature and mass gradients in the vertical direction are maintained, which translates into higher heat and mass transfer rates within the cavity. In addition, for higher N values, the heat and mass transfer rates by convection mechanism are found to build up since the solutal buoyancy force is aiding the flow. This condition is reflected on the velocity magnitude of the central vortex, which is noted to register a higher value. For positive values of buoyancy ratio parameter ($N > 0$), higher velocity magnitudes for the clockwise central vortex are observed by an increase in $|\Psi_{\min}|$ value. In this scenario, the solutal buoyancy force enhances energy transport since it acts in the same direction of the lid-driven wall. Fig. 8 demonstrates that negative values of N indicate a scenario of opposing flow condition where the net buoyancy force is weakened. Upon incorporating larger negative N values, the flow becomes further weakened by the opposing thermal and mass buoyancy forces. Consequently, the main vortex slows down and eventually breaks up into two prime vortices filling most of the cavity. Also, the flow magnitude is illustrated to significantly reduce in the lower half of the cavity. Accordingly, the overall heat transfer occurs primarily

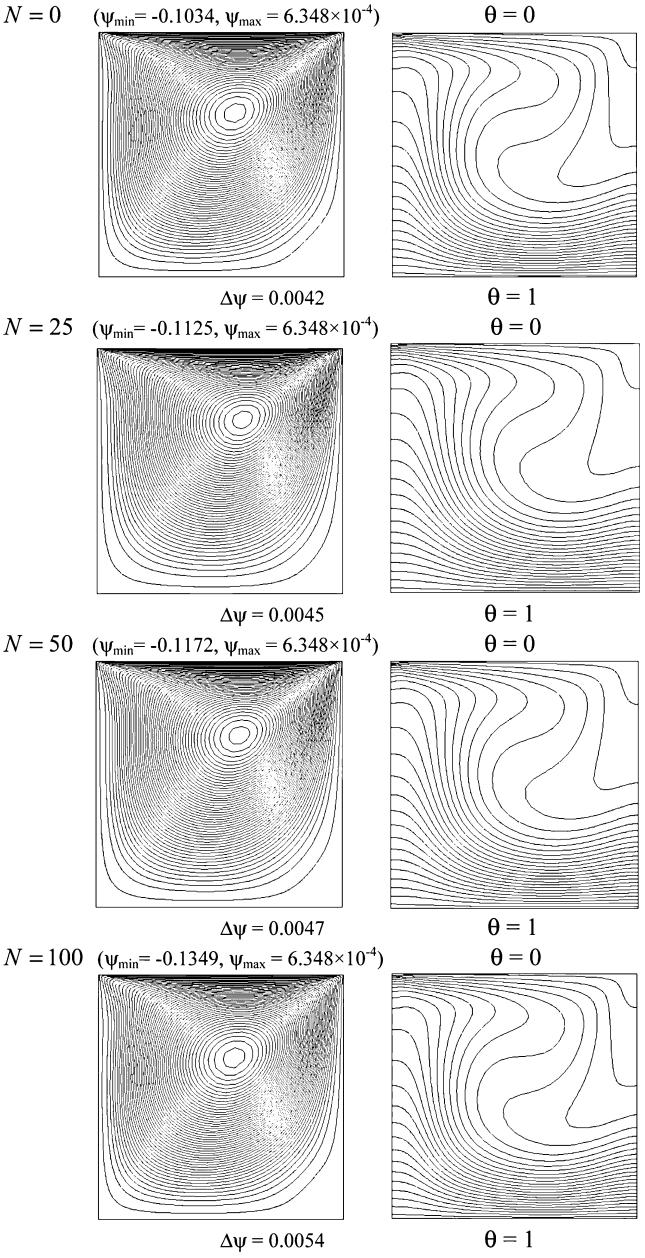

Fig. 7. Effect of positive N values on the streamlines and isotherms for $Re = 100$, $Ri = 0.01$, and $Le = 1$.

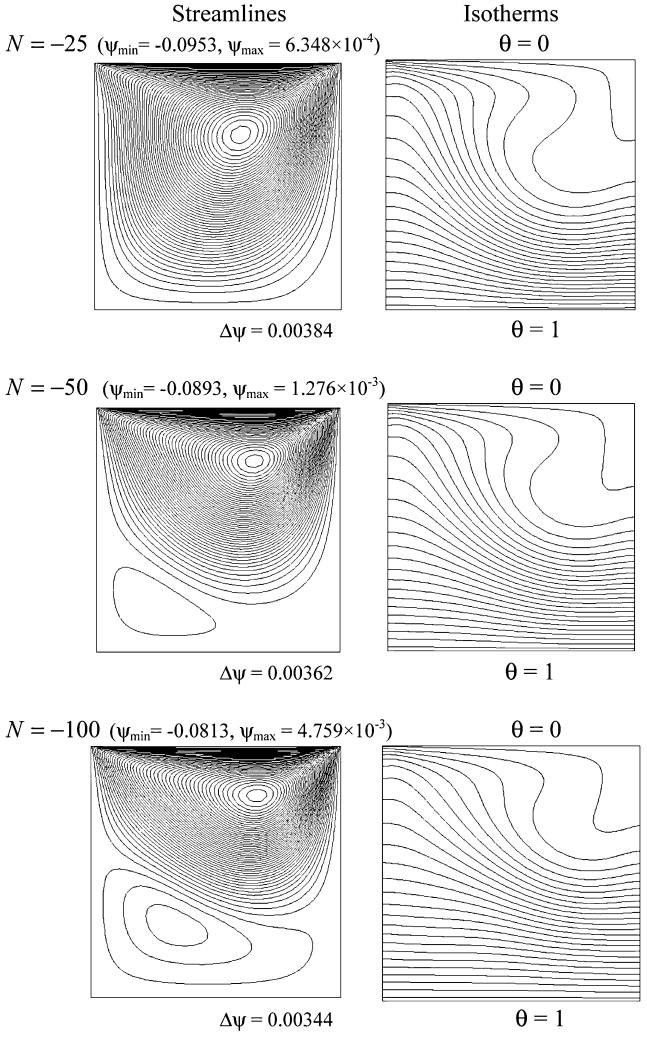

Fig. 8. Effect of negative N values on the streamlines and isotherms for $Re = 100$, $Ri = 0.01$, and $Le = 1$.

by conduction in the center and bottom regions of the cavity. This is depicted by the linear temperature stratification in such regions. The top region, however, remains affected by the convection heat transfer regime owing to the mechanical effect of the sliding lid.

Fig. 9 shows the variation of the temperature and velocity profiles along the mid-sections of the cavity for $Re = 100$, $Ri = 0.01$, $Le = 1$ and various values of the buoyancy ratio parameter N. For large negative values of N (opposing flow), the temperature distribution in most of the cavity is shown to retain similar behavior to that of a pure conduction regime except near the sliding top wall. In addition, Fig. 9 illustrates that the velocity component U and V exhibits higher values along their respective walls for positive N values compared to their negative counterparts. This could be attributed to the fact that the mass (concentration) buoyancy force is assisting the flow for the positive N values. The areas of relatively high velocity magnitudes manifest high transport rate, which are important in drying applications where high species transfer is sought.

The work is wrapped by presenting the effect of the buoyancy ratio parameter N on average Nusselt number evaluated at the bottom wall of the cavity for $Le = 1$. As shown in Fig. 10, the results clearly indicate that the increase in the positive value of N (aiding flow) augments the heat and mass transfer in the cavity. This is noted by the rapid increase in the average Nusselt number (or the Sherwood number). The opposite can be observed once N marches in the negative direction (opposing flow). This can be attributed to the fact that the solutal buoyancy force in this situation is opposing the mechanical effect of the moving wall. The magnitude of N value is more pronounced on Nusselt number predictions for $Ri = 0.01$. It is obvious that the combined effect of sliding wall and solutal buoyancy force intensifies heat transfer by convection within the cavity. Such effect is reduced when the speed of the sliding lid is reduced for Ri equals to 1 and 10, respectively. Apparently, conduc-

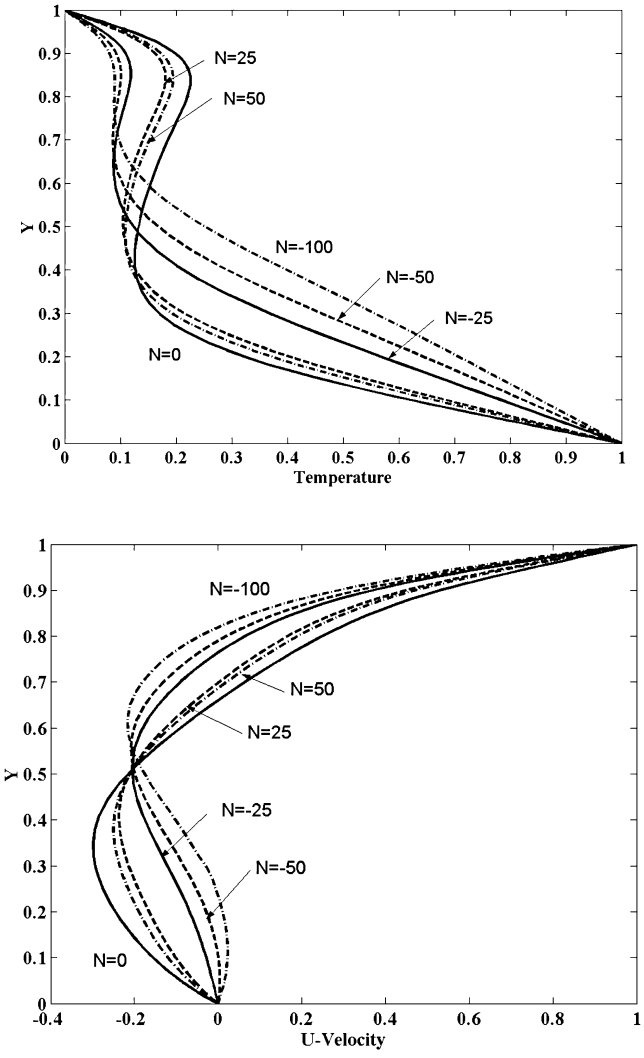

Fig. 9. Effect of N on the temperature and velocity profiles along the mid-section of the cavity for $Re = 100$, $Ri = 0.01$ and $Le = 1$.

tion heat transfer regime becomes dominant for $N < -15$ due to the suppression in the convection effect. Overall, average Nusselt number is observed to approach an asymptotic value around $|N| = 100$, which establishes upper and lower bounds for the predicted Nusselt number values. It also defines the operating range where buoyancy ratio number can be considered effectively in determining the level of heat and mass transfer augmentation.

5. Summary and conclusions

The current investigation is concerned with heat and mass transfer in a lid-driven cavity filled with a binary fluid of $Pr = 1$ that operates under combined temperature and mass (concentration) gradients. The results of this work illustrate that heat transfer and mass transfer characteristics inside the cavity are enhanced for low values of the Richardson number Ri due to the dominant effect of the mechanical effect induced by the moving lid. Thinner mass boundary layers are observed along the bottom wall of the cavity with an increase in Lewis number resulting in higher mass transfer rates. However, Lewis number has insignificant effect on the isotherms and streamlines for small Richardson numbers. Positive buoyancy ratio number is found to augment both heat and mass transfer rates inside the cavity while negative buoyancy ratio deteriorates the effect of the buoyancy ration. Consequently, the main vortex slows down and eventually breaks up into two prime vortices filling most of the cavity. The predicted average Nusselt number obtained at the bottom wall was presented against the buoyancy ratio number for fixed Ri values. The average Nusselt number is observed to establish upper and lower bounds for the predicted Nusselt number values. Thus, the results establish the range of the operating buoyancy ratio parameter where transport activities can be manipulated. Further work is recommended to extend the current investigation to a wider range of the Richardson number. This shall aid in examining the contribution weight of the dimensionless variables in augmenting the heat and mass transfer in the present configuration.

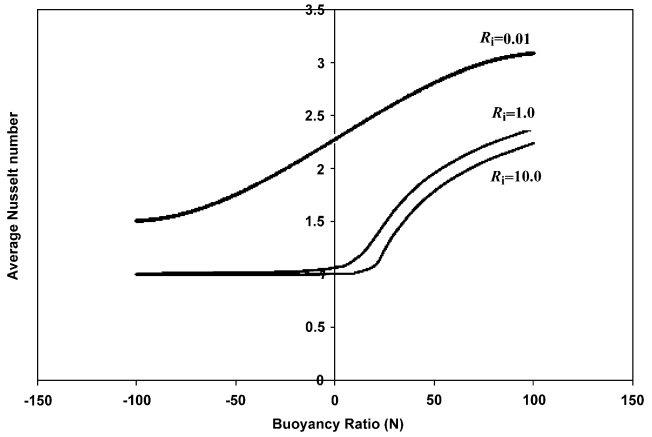

Fig. 10. Effect of the buoyancy ratio number on the average Nusselt number for $Le = 1$.

References

[1] M. Hasan, S. Mujumdar, Simultaneous mass and heat transfer under mixed convection along a vertical cone, Energy Res. 9 (1985) 129–140.
[2] S. Ostrach, Natural convection with combined driving forces, Physico Chem. Hydrodyn. 1 (1980) 233–247.
[3] A. Mohamad, R. Viskanta, Convective flow and heat transfer in a lid-driven shallow cavity with buoyancy, ASME/JSME Thermal Engrg. Proc. 1 (1991) 89–96.
[4] R. Ben Mansour, R. Viskanta, Fluid flow and heat transfer in shallow cavities driven by shear and buoyancy, Fund. Mixed Convection, ASME HTD 213 (1992) 31–42.
[5] O. Aydin, Aiding and opposing mechanisms of mixed convection in a shear- and buoyancy-driven cavity, Int. Commun. Heat Mass Transfer 26 (1999) 1019–1028.
[6] T.-H. Hsu, P.-T. Hsu, C.-K. Chen, Thermal convection of micropolar fluids in a lid-driven cavity, Int. Commun. Heat Mass Transfer 22 (1995) 189–200.
[7] O. Aydin, W.-J. Yang, Mixed convection in cavities with a locally heated lower wall and moving sidewalls, Numer. Heat Transfer, Part A 37 (2000) 695–710.
[8] O.V. Trevisan, A. Bejan, Combined heat and mass transfer by natural convection in a vertical enclosure, ASME J. Heat Transfer 109 (1987) 104–112.
[9] Y. Kamotani, L.W. Wang, S. Ostrach, H.D. Jiang, Experimental study of natural convection in shallow enclosures with horizontal temperature and concentration gradients, Int. J. Heat Mass Transfer 28 (1985) 165–173.

[10] J. Lee, M.T. Hyun, G.W. Kim, Natural convection in confined fluids with horizontal temperature and concentration gradients, Int. J. Heat Mass Transfer 31 (1988) 1969–1977.
[11] P. Ranganathan, R. Viskanta, Natural convection in a square cavity due to combined driving forces, Numer. Heat Transfer, Part A 14 (1988) 35–59.
[12] S. Mergui, D. Gobin, Transient double diffusive convection in a vertical enclosure with asymmetrical boundary conditions, ASME J. Heat Transfer 122 (2000) 598–601.
[13] H. Han, T.H. Kuehn, A numerical simulation of double diffusive convection in a vertical rectangular enclosure, Heat Transfer Convective Flows, ASME HTD 107 (1989) 149–154.
[14] J.A. Weaver, R. Viskanta, Natural convection in binary gases due to horizontal thermal and solutal gradients, ASME J. Heat Transfer 113 (1991) 141–147.
[15] H.C. Kuhlmann, M. Wanschura, H.J. Rath, Flow in two sided lid-driven cavities: non-uniqueness, instabilities, and cellular structures, J. Fluid Mech. 336 (1997) 267–299.
[16] N. Alleborn, H. Raszillier, F. Durst, Lid-driven cavity with heat and mass transport, Int. J. Heat Mass Transfer 42 (1999) 833–853.
[17] A. Bejan, Convection Heat Transfer, second ed., John Wiley & Sons, New York, 1995.
[18] O.V. Trevisan, A. Bejan, Natural convection with combined heat and mass transfer buoyancy effects in a porous medium, Int. J. Heat Mass Transfer 28 (1985) 1597–1611.
[19] O.V. Trevisan, A. Bejan, Mass and heat transfer by high Rayleigh number convection in a porous medium heated from below, Int. J. Heat Mass Transfer 30 (1987) 2341–2356.
[20] B. Goyeau, J.-P. Songbe, D. Gobin, Numerical study of double-diffusive natural convection in a porous cavity using the Darcy–Brinkman formulation, Int. J. Heat Mass Transfer 39 (1996) 1363–1378.
[21] M. Mamou, P. Vasseur, E. Bilgen, Multiple solutions for double diffusive convection in a vertical porous enclosure, Int. J. Heat Mass Transfer 38 (1995) 1787–1798.
[22] P.M. Gresho, R.L. Lee, R.L. Sani, On the time-dependent solution of the incompressible Navier–Stokes equations in two and three dimensions, in: Recent Advances in Numer. Methods and Fluids, vol. 1, Pineridge, Swansea, UK, 1980, pp. 27–81.
[23] C. Taylor, P. Hood, A numerical solution of the Navier–Stokes equations using finite-element technique, Comput. Fluids 1 (1973) 73–89.
[24] E. Barragy, G.F. Carey, Stream function-vorticity driven cavity solution using p finite element, Comput. Fluids 26 (1997) 453–468.
[25] R. Screiber, H.B. Keller, Driven cavity flows by efficient numerical techniques, J. Comput. Phys. 49 (1983) 310–333.
[26] U. Ghia, K.N. Ghia, C.T. Shin, High-*Re* solutions for incompressible flow using the Navier–Stokes equations and a multigrid method, J. Comput. Phys. 48 (1982) 387–411.
[27] O. Botella, R. Peyret, Benchmark spectral results on the lid-driven cavity flow, Comput. Fluids 27 (1998) 421–433.
[28] C.-H. Bruneau, C. Jouron, An efficient scheme for solving steady incompressible Navier–Stokes equations, J. Comput. Phys. 89 (1990) 389–413.
[29] G.B. Deng, J. Piquet, P. Queutey, M. Visonneau, Incompressible flow calculations with a consistent physical interpolation finite volume approach, Comput. Fluids 23 (1994) 1029–1047.